



RESEARCH ARTICLE

10.1029/2021AV000395

Rapid Response to the 2019 Ridgecrest Earthquake With Distributed Acoustic Sensing

Zefeng Li^{1,2} , Zhichao Shen² , Yan Yang² , Ethan Williams² , Xin Wang² , and Zhongwen Zhan² ¹Laboratory of Seismology and Physics of Earth's Interior, School of Earth and Space Sciences, University of Science and Technology of China, Hefei, Anhui, China, ²Seismological Laboratory, Division of Geological and Planetary Sciences, California Institute of Technology, Pasadena, CA, USA

Key Points:

- The first emergency response to a major earthquake with distributed acoustic sensing (DAS) proves great potential for aftershock monitoring
- Application of template matching to DAS detects six-fold more aftershocks than the standard Southern California Seismic Network catalog
- The enhanced catalog reveals markedly active aftershocks on the crosscutting faults near the M 6.4 and M 7.1 epicenters

Supporting Information:

Supporting Information may be found in the online version of this article.

Correspondence to:

Z. Li and Z. Zhan,
zefengli@ustc.edu.cn;
zwzhan@caltech.edu

Citation:

Li, Z., Shen, Z., Yang, Y., Williams, E., Wang, X., & Zhan, Z. (2021). Rapid response to the 2019 Ridgecrest earthquake with distributed acoustic sensing. *AGU Advances*, 2, e2021AV000395. <https://doi.org/10.1029/2021AV000395>

Received 15 JAN 2021

Accepted 25 MAY 2021

Author Contributions:

Conceptualization: Zefeng Li, Zhichao Shen, Zhongwen Zhan
Data curation: Zhichao Shen, Ethan Williams, Xin Wang
Formal analysis: Zefeng Li, Zhichao Shen, Yan Yang
Funding acquisition: Zhongwen Zhan
Supervision: Zhongwen Zhan
Writing – original draft: Zefeng Li, Zhichao Shen, Zhongwen Zhan
Writing – review & editing: Zefeng Li, Zhichao Shen, Yan Yang, Ethan Williams, Xin Wang, Zhongwen Zhan

© 2021. The Authors.

This is an open access article under the terms of the [Creative Commons Attribution-NonCommercial License](#), which permits use, distribution and reproduction in any medium, provided the original work is properly cited and is not used for commercial purposes.

Abstract Rapid seismic deployments after major earthquakes often produce critical data for characterizing postseismic processes. Taking advantage of pre-existing optical fibers, the recently emerging distributed acoustic sensing (DAS) technology can quickly establish ultra-dense seismic arrays after the mainshocks. Here we present the first example of such a rapid-response experiment using four telecommunication fiber optic cables near the 2019 M 7.1 Ridgecrest earthquake in California. By applying template matching to the Ridgecrest DAS array, we detected 6 times more aftershocks than the standard catalog within the three-month period. The enhanced catalog reveals abundant aftershocks on multiple crosscutting faults near the epicenters of the mainshock and the M 6.4 foreshock. Given the widespread fiber optic networks around the world, DAS has the potential to deliver fast and high-resolution aftershock monitoring and promote better understanding of earthquake physics.

Plain Language Summary After a large earthquake, geophysicists often deploy instruments around the event as quickly as possible to monitor the aftershocks, to collect critical measurements about earthquake physics. The recently emerging distributed acoustic sensing (DAS) technology can take advantage of pre-existing optical fibers to establish ultra-dense seismic arrays within hours. We present the first example of a rapid response DAS experiment after the 2019 M 7.1 Ridgecrest earthquake in California. We show that the Ridgecrest DAS array detected 6 times more aftershocks than in the conventional catalog and performed similarly to the relatively dense local network. Because fiber optic networks are widespread around the world, DAS can be potentially a transformative tool for rapid aftershock monitoring and contributes to better understanding of earthquake physics.

1. Introduction

Large earthquakes are usually followed by numerous aftershocks which reflect transient postseismic processes. Significant aftershocks may cause secondary hazards for buildings and infrastructure that are already weakened by the mainshock. At small odds (typically 5%), a more destructive event could occur in the “aftershock” sequence, posing one of the biggest challenges in real-time seismic hazard forecasting (Gulia & Wiemer, 2019; Reasenber & Jones, 1990; Roeloffs & Goltz, 2017). Close monitoring and high-resolution characterization of aftershock sequences is therefore important for tracking temporal evolution of subsequent earthquake hazards and improving our understanding of earthquake physics and postseismic deformation.

While regional and global permanent seismic networks have been successful in monitoring moderate to large earthquakes, their spatial coverages are often insufficient near large earthquakes to monitor the aftershocks in high resolution. As a result, rapid deployment of near-field seismic instruments in response to large earthquakes is essential. Speed and coverage are two key factors for such deployment campaigns. Since postseismic processes tend to decay rapidly after the mainshock, delays in deployment could lead to an irreversible loss of critical measurements. Furthermore, poor spatial sampling of seismic wavefields can impact the detection capability for small earthquakes as well as the accuracy of various source parameters.

Traditionally, broadband and short-period seismometers are used in earthquake rapid responses and have achieved great success in advancing our knowledge about aftershock processes. The deployment logistics, however, are burdensome and require a relatively large team, which limits the array density and response

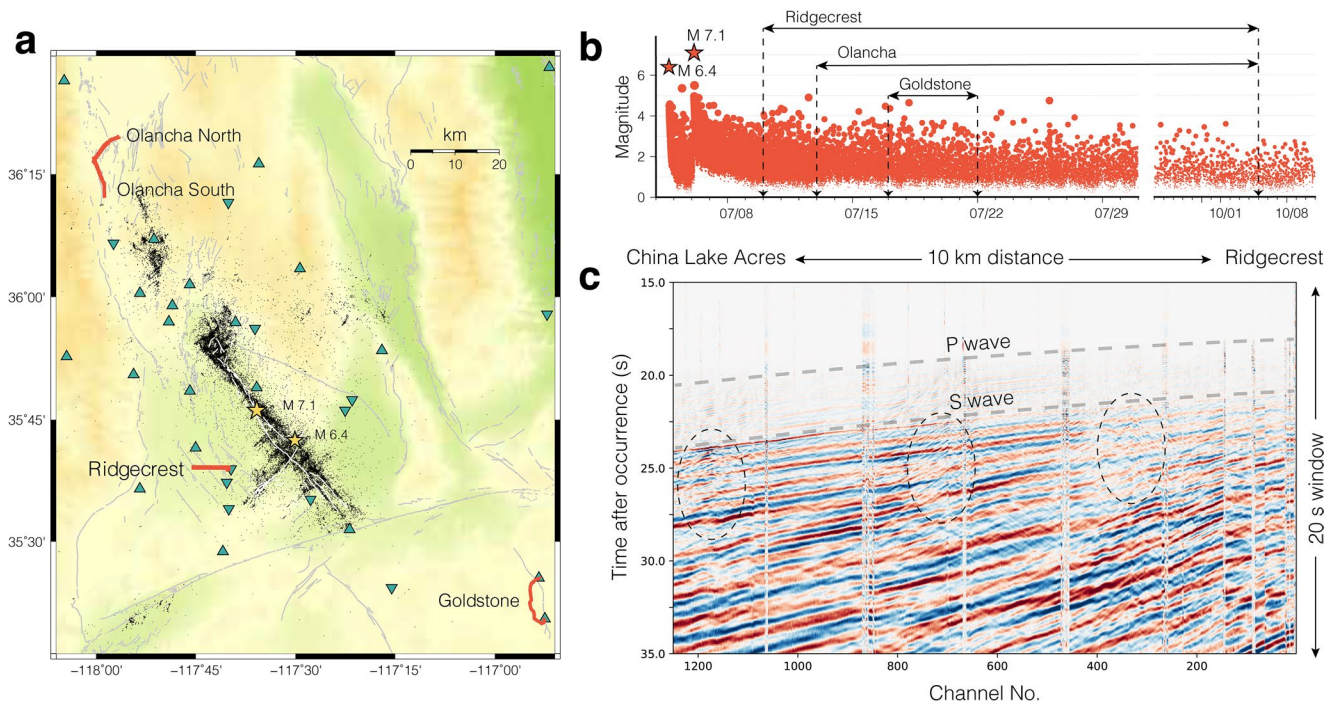


Figure 1. Rapid response with distributed acoustic sensing (DAS) based on city-scale optic fiber networks to the 2019 M 7.1 Ridgecrest earthquake. (a) Map of aftershocks (black dots) and DAS arrays (red lines) started after the Ridgecrest earthquake. Two yellow stars mark the locations of the M 7.1 and M 6.4 events. Green triangles and inverse triangles are CI and other permanent partner stations in the Southern California Seismic Network. Light gray lines represent the major faults in the region. White lines represent the surface rupture of M 7.1 event. (b) Timeline of the DAS array operation during the aftershock sequence in the Southern California Earthquake Data Center (SCEDC) catalog. (c) The Ridgecrest DAS recordings of the wavefield of an M 3.9 aftershock on July 27, 2020 (SCEDC event id 38653975). Channels are sorted from China Lake Acres (western terminus) to Ridgecrest (eastern terminus). The dashed circles mark scattered waves possibly associated with unmapped faults underneath the array.

speed. In the last decade, standalone nodal sensors that integrate memory storage and battery have become common for rapid response (Beskardes et al., 2019; Catchings et al., 2020; Pankow et al., 2021). Thanks to their easy installation, nodes have enabled earthquake monitoring with a massive number of sensors (also known as large-N) for the first time (Fan & McGuire, 2018; Inbal et al., 2015, 2016; Li, 2018).

Recently, distributed acoustic sensing (DAS) has emerged as another novel technology to obtain massive numbers of seismic sensors at relatively low cost (Lindsey et al., 2017; Zhan, 2020). DAS can transform an optical fiber into thousands of meter-spaced seismic sensors by measuring the backscattered light from intrinsic fiber impurities. Recent applications have demonstrated that DAS can record high-fidelity wavefields from local and regional earthquakes (Lindsey et al., 2017; H.F. Wang et al., 2018). The ultra-dense recordings provide unprecedented resolution for earthquake monitoring (e.g., Li & Zhan, 2018) and subsurface imaging (Lindsey et al., 2019). However, rapid response after a major earthquake demands not only high resolution but also fast installation; the potential of DAS as a rapid response system has not been fully explored before.

Here we present the first example of using DAS for earthquake rapid response after the 2019 M 7.1 Ridgecrest event (Figure 1). The Ridgecrest earthquake occurred on July 6, 2019 at UTC 03:19:53, preceded by an M 6.4 foreshock. In the days following the earthquake, we accessed multiple pre-existing telecommunication fiber optic cables around the source region and deployed four DAS units to convert a total of 55 km cables into a network with over 6,000 seismic sensors. To demonstrate the monitoring capability of DAS, here we focus on the Ridgecrest DAS array given its unique location near the aftershock zone. The Ridgecrest DAS array started recording 4 days after the M 7.1 event and was operated until October 4, 2019. It turned a 10 km long optical fiber in the City of Ridgecrest (Figure 1) into 1,250 channels with 8 m spacing. It recorded high-fidelity wavefields from many Ridgecrest aftershocks, providing a unique opportunity to

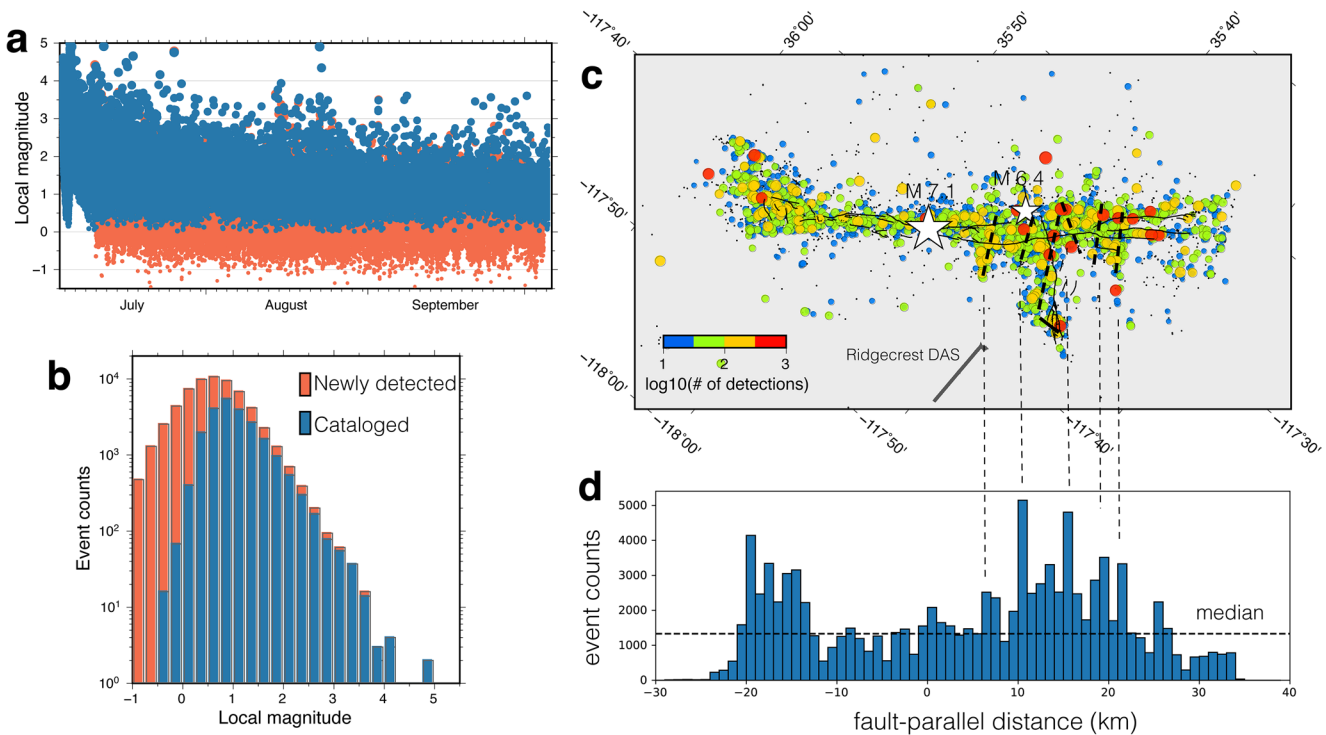


Figure 2. Aftershock sequence improved by template matching on the Ridgecrest distributed acoustic sensing (DAS) array. (a) Aftershock temporal sequence from cataloged events (blue dots) and newly detected events from DAS (red dots). Only the ones with calibrated magnitude are shown. (b) Magnitude distribution of cataloged (blue) and newly detected events with calibrated magnitude (red). (c) The number of new detections per template, with both magnitude calibrated and uncalibrated considered. Dot size is logarithmically proportional to the detections. Black dashed line mark the cross faults following the illustration by Shelly. (d) Histogram of newly detected events along the main fault.

evaluate the potential of DAS in aftershock monitoring and benchmark its performance with the high-quality conventional local network as part of the Southern California Seismic Network (SCSN; Figure 1a).

2. Enhanced Aftershock Monitoring With DAS

We apply template matching to the DAS data to detect small events missing in the standard SCSN catalog (Figure S1) (Peng & Zhao, 2009; Ross, Idini et al., 2019). Li and Zhan (2018) applied template matching to the PoroTomo DAS array in the Brady Hot Spring geothermal field and detected >100 events well below noise level with 5 template events, thanks to the cross-correlation stacking from a massive number of DAS channels. Here, we use 22,465 aftershocks from the SCSN catalog during the same period of time as template candidates. The signal-to-noise (SNR) ratio is calculated on each channel with a noise window 5.5–0.5 s before S arrivals and a signal window 0–5 s after the S arrivals. The final template library consists of 9,318 events with SNR > 5 dB on at least 200 DAS channels. The waveform windows for cross-correlation are 1 s before and 5 s after the S arrivals. Cross-correlation of the templates with the continuous data leads to about 37 million hourly traces averaged over the array. We use a peak threshold of 10 times the median absolute deviation above the median noise level on hourly cross-correlations and remove duplicate detections from different templates. Finally 133,453 events are detected, which are 6 times more than those in the SCSN catalog (Figure 2).

Likely due to the strong traffic noise near the fiber path, the signals for $M < 2$ events on individual channels are in general below the noise floor (Figure S2). To calibrate the magnitude for the newly detected small events, we use the nearby broadband seismometers. While the small events are usually not detected by multiple broadband stations to be in the catalog, they are mostly visible at one or two stations. The calibration procedure follows Shelly (2020): we first calculate the amplitude ratio of body waves between the templates and the newly detected events, and then convert it to local magnitude (ML) difference empirically using

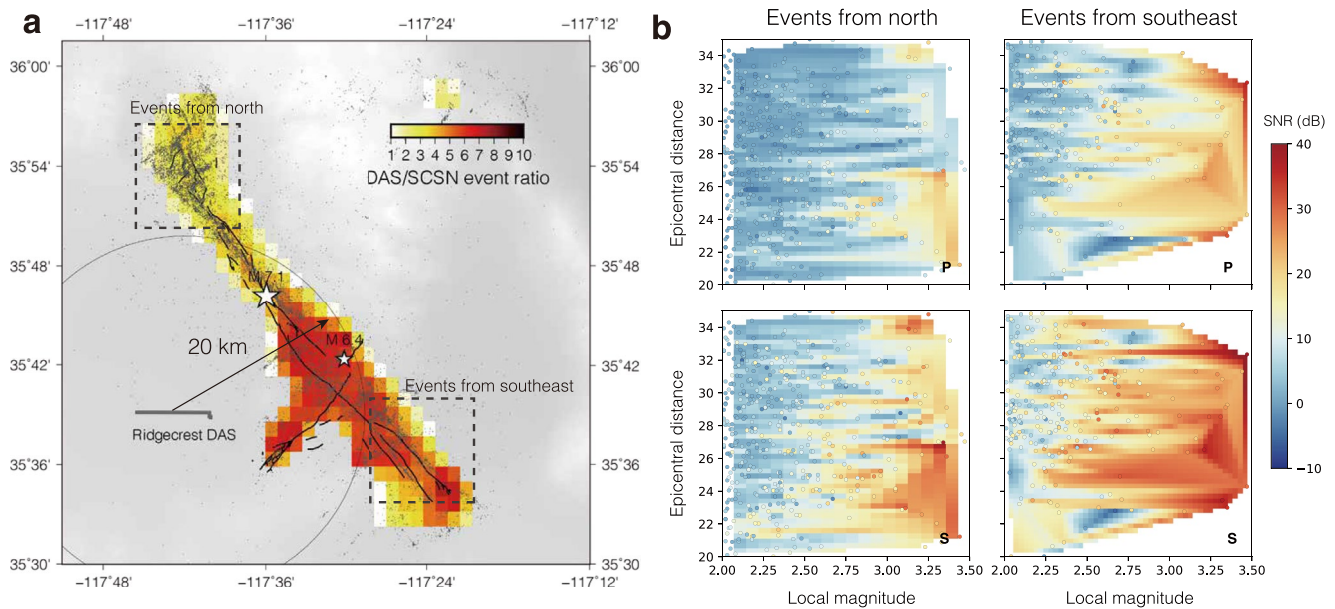


Figure 3. The impact of distance and back azimuth on distributed acoustic sensing (DAS) detection capability. (a) Ratio of detected events on DAS to the Southern California Seismic Network cataloged events in 1 km bin size. The circle marks the range of 20 km from the DAS center. (b) Comparison of P and S wave signal-to-noise (SNR) of events from the north and southeast (boxes in A). The dots represent individual events, color coded by SNR, which are used to interpolate the background colormap. In similar ranges of magnitude and distance, the southeastern events have higher SNR than the northern ones, demonstrating the azimuth-dependent effect on DAS.

$ML_2 = ML_1 + 0.831 \log_{10} \frac{A_2}{A_1}$. The results show that the magnitudes of most newly detected events are $ML_{-1} \sim ML_1$ (Figure 2). We do not relocate the new events like other broadband template matching applications (Ross, Idini et al., 2019; Shelly, 2020) due to the limited azimuth coverage of the DAS array. Instead, we assign the template event locations to the newly detected events, given that previous studies have shown their locations are likely near the corresponding templates (Meng & Peng, 2014; Peng & Zhao, 2009; Ross, Idini et al., 2019).

From the enhanced catalog, we observe significantly higher rates of aftershocks in the northwest terminus and the middle segment of the M 7.1 rupture (Figure 2d). Previous template-matching catalogs (Ross, Trugman et al., 2019; Shelly, 2020) also showed that the northwest terminus are particularly active and likely have multiple sets of shallow orthogonal faults (Figure S3). Around the middle segment of the M 7.1 rupture, there exist several tightly spaced southwest (SW) striking faults that are perpendicular to the M 7.1 rupture but subparallel to the SW limb of the M 6.4 rupture (Shelly, 2020). These crosscutting faults primarily extend to the SW side of the main rupture. In our DAS catalog, we are able to recover many more events on these crosscutting faults (Figure S3), thanks to the DAS's proximity to the section. By accounting the number of events along the main rupture, these faults show up as spikes on the histogram (Figure 2d). This indicates that the cross-cutting faults produce a large fraction of aftershock activities, likely suggesting a higher rate of aftershock production than along the main fault. It remains unclear whether or not this is a combined effect with the relatively large stress drop of the M 7.1 event (Wang & Zhan, 2020) and fresh activation of the cross-cutting faults during and/or after the mainshock (Shelly, 2020).

3. Impact Factors of DAS in Earthquake Rapid Response

The Ridgecrest DAS experiment provides an opportunity to evaluate the various factors that can impact DAS's performance and need to be considered in future responses. For example, mostly due to the decay of signals, the Ridgecrest DAS array has optimal detection capability (DAS/SCSN event ratio > 5) within about 20 km from the array center (Figure 3a). To evaluate the variations of detectability within the array, we calculate the SNRs of all template events on each channel (Figure S4). In addition to fiber service loops

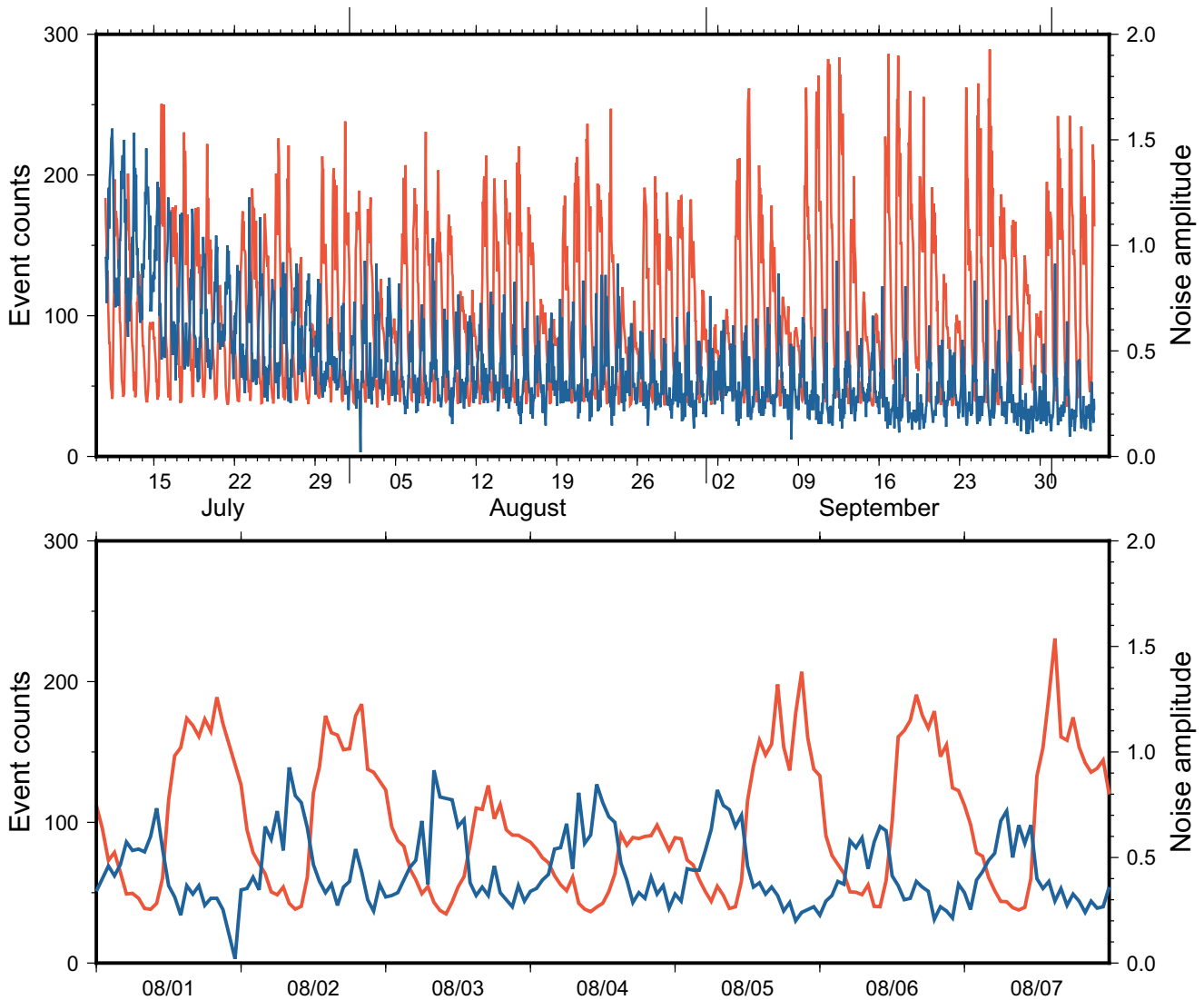


Figure 4. The impact of near-fiber traffic noise on distributed acoustic sensing (DAS) detection capability. (a) Hourly detected events (blue) and hourly average noise amplitude (red) over the 3 month recording period. (b) Zoom-in plot for the first week of August 2019, showing anti-correlation between detected events (blue) and noise amplitude (red). (c) Amplitude spectra of hourly event counts (blue) and Southern California Seismic Network cataloged events (gray), and the hourly average noise (red). Both noise spectrum and DAS event spectrum shows periodicity around 1 week, 24, 12, and 8 h, demonstrating the impact of noise on earthquake detectability.

with low ground coupling, the overall variations show a significant channel dependence. The number of detectable events (defined as $\text{SNR} > 5$ dB) varies between 4,000 to 6,000, a change of $\sim 20\%$ relative to the mean. A similar range of variation is also shown in the SNR at 75 percentile of all events. Furthermore, we observe no significantly higher SNRs on the eastern section of the fiber which is generally closer to the earthquakes, likely because the fiber is relatively short and the SNR windows consist of less rapidly decaying scatter and surface waves.

Given the linear geometry of the Ridgecrest DAS array, the directional sensitivity of DAS also affects the aftershock SNRs (Benioff, 1935; Zhan, 2020). To examine its effect on earthquake detectability, we measure the SNRs of the aftershocks to the north (incident angle with respect to the array from 80° to 110°) and the southeast (incident angle with respect to the array from -40° to 20°) (Figure 3b) with similar magnitudes (M_2 - $M_{3.5}$) and epicentral distance (20–35 km). Figure 4c shows that the SNRs of P and S waves from the southeast are systematically higher (~ 5 – 10 dB) than those from the north. This is consistent with theoretical prediction that waves perpendicular to DAS arrays have minimal amplitudes. The directional

earthquake detection capability of DAS needs to be taken into account in rapid responses when possible, for example by using sections of cable with changing orientations.

The detection capability is also modulated temporally by cultural noise near the fiber path (Figure 4). The Ridgecrest DAS array was along a major road (U.S. Route 395 Business/West Inyokern Road) and recorded the strong traffic noise (Wang et al., 2020). The diurnal variations of traffic noise significantly modulated the DAS earthquake detection capability. In the first week of August, for example, there are 100–200 events per hour detected at night, but only ~50 events per hour during the daytime, anti-correlated with the noise amplitude (Figure 4b). This change at a factor of 2–4 is much larger than that of the SCSN network (Atef et al., 2009), because optical fibers in cities are much closer to human and industrial activities than the SCSN stations. Spectral analysis of the hourly event counts against the hourly DAS noise amplitudes shows not only the 24 h periodicity but also other human-related periodicities, e.g., weekly, 12 h, and 8 h. These periodicities further demonstrate the high impact of cultural noise on DAS detectability.

4. Discussion

In response to the 2019 M 7.1 Ridgecrest earthquake, we took advantage of the pre-existing telecommunication fiber optic networks to rapidly build aftershock monitoring systems in the vicinity of the sequence. We detected numerous small aftershocks on the DAS recordings, 6 times more than those in the standard SCSN catalog. The improved catalog reveals many more aftershocks on the secondary SW-striking faults cross-cutting the middle segment of the main rupture (Ross, Trugman et al., 2019; Shelly, 2020), suggesting these unusually active small faults may take up a significant proportion in the aftershock population. We learn that the Ridgecrest DAS array has an optimal detectability radius of about 20 km and that the azimuth dependence of body wave amplitudes strongly impacts the detection of events. The anthropogenic noise near the fiber can lead to a factor of 2–4 difference in the number of new detections in the day and night times. As the first attempt, the Ridgecrest DAS arrays will serve as a useful reference for future DAS rapid response campaigns.

It is noteworthy that Ridgecrest is a well instrumented areas within the SCSN (Hauksson et al., 2020), with station spacing of 10–20 km. Our catalog constructed from the 10 km DAS array is substantially better than the standard catalog and is comparable to the Ross, Trugman et al. (2019) and Shelly (2020) template matching catalogs. To evaluate the performance of a similar DAS array in less instrumented areas, we test how the final catalog changes with only the bigger template events. With 147 $M > 3$ templates, the Ridgecrest DAS array produces 49,936 detections (a 340 times increase); with 482 $M > 2.5$ templates, it produces 61,155 detections (a 127 times increase). This demonstrates that, in areas without a high-quality permanent seismic network, DAS can be of even greater value and thus play a comparatively more important role in seismic monitoring.

DAS has several outstanding advantages as a rapid response system (Figure 5). First, DAS provides large-N monitoring capability (e.g., Catchings et al., 2020) with meter-scale spacing and unaliased recording of the higher frequency wavefields. The dense spatial sampling offers high-resolution earthquake detectability, as demonstrated in this study. Also, recent results have shown that ambient noise correlation on DAS channels can be used to obtain high-resolution subsurface structures (Cheng et al., 2021; Dou et al., 2017). Yan et al. (2021) applied ambient noise tomography to the Ridgecrest array and observed strong lateral variations of the velocity structures that correlate well with shaking intensity. The dense spatial sampling is also valuable for mapping previously unknown faults (Jousset et al., 2018; Lindsey et al., 2019).

DAS can make use of the widespread inland and offshore fiber optic networks for rapid response. Without the need to deploy cables from scratch, installation of DAS can be as convenient as connecting a DAS interrogator unit to fiber terminus and power supply. Transportation and deployment of a large number of conventional seismometers or nodal sensors requires a relatively large team, more permitting, and days of time, whereas DAS can be installed by a two-person team within hours if fiber access is ready. Swift DAS response to major earthquakes could be critical to preserve perishable information soon after the mainshock. Moreover, DAS allows real-time data telemetry because all the data from the channels distributed over tens of kilometers along cable are processed and collected at the terminal DAS system. Therefore, DAS data can be uploaded to cloud computer centers in near real-time and integrated into the existing seismic networks

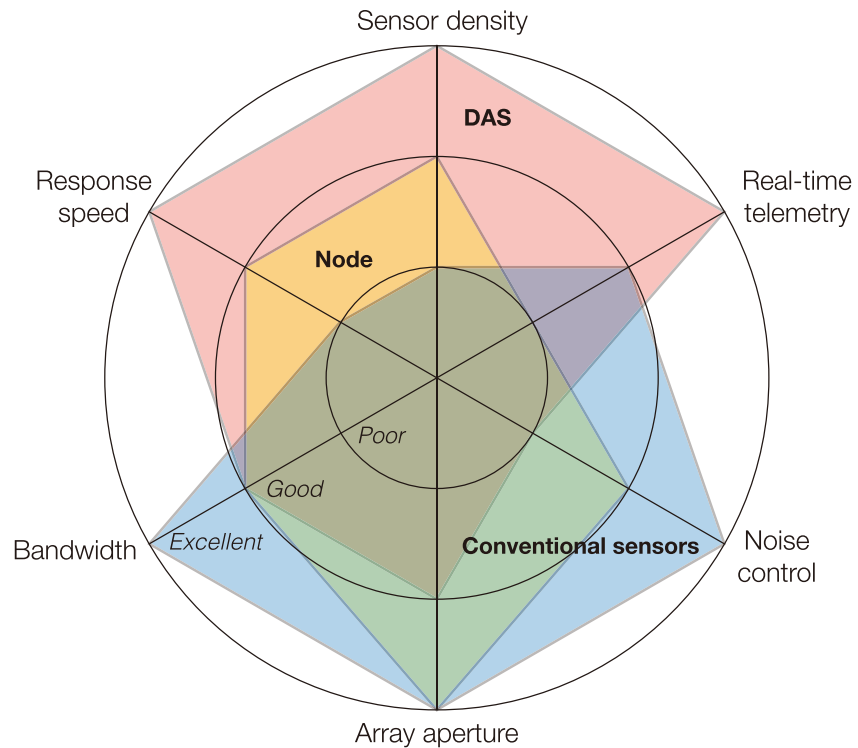


Figure 5. Qualitative comparison of seismic instruments for earthquake rapid response, scored in terms of response speed, sensor density, real-time telemetry, noise control, bandwidth, and array aperture. Conventional sensors, including broadband and short-period seismometers, are advantageous in frequency bandwidth and station quiescence but disadvantageous in response speed and sensor density. Nodal sensors can provide ultra-dense and wide coverage and relatively fast response, but cannot operate in real-time due to battery and storage limitation. Distributed acoustic sensing provides densest coverage, fastest response time, and capability for real-time telemetry, thus would be a beneficial addition to rapid response systems. The performance levels (poor, good, and excellent) are approximate in general scenarios and exceptions might exist.

that are also hosted on cloud (e.g., SCSN). In practice, the major challenge lies in processing large volume of data, which calls for leveraging the power of parallel computing and efficient down-sampling algorithms. Despite this, DAS appears to be the only large-N technology with plausible real-time telemetry options, critical for closely tracking ongoing aftershock sequences.

With the strengths in sensor density, response speed, and real-time telemetry, DAS can be combined with other technologies to maximize the capability of rapid response systems (Figure 5). First, as shown in the Ridgecrest example, fiber optic networks are often along major roads, resulting in elevated noise level and strong diurnal noise fluctuation (Figure 4). In comparison, the locations of standalone seismometers can be carefully chosen to stay away from anthropogenic sources. Therefore, complementing DAS with standalone seismometers may reduce the impact from cultural noise. Especially, the quiet seismometers can provide high-fidelity amplitude information for the very small events, which enables magnitude calibration of the small events detected by DAS. In addition, limited by the decay of backscattered light, so far a single DAS array cannot extend beyond several tens of km, which is insufficient to cover aftershock zones of large events. On the other hand, nodal and conventional seismometers can be scattered around to form broader apertures. Hence, it could be preferable to deploy DAS near critical zones, such as faults, for high-resolution observations, and scatter seismometers around for wide-azimuth coverage. Third, similar to nodal sensors and short-period seismometers, DAS is most sensitive at high frequencies (~5 Hz), even though some tele-seismic waves up to tens of seconds can be recorded (Lindsey et al., 2020; Yu et al., 2019). Broadband seismometers can be used to complement the bandwidth to help determination of various source parameters, such as magnitude and focal mechanisms. Therefore, integration of multiple types of instruments could be essential to build a well-rounded rapid response system (Figure 5).

With pervasive fiber optic networks around the world, the use of DAS as a standard rapid response tool appears attractive. With the equipment and fiber access prepared ahead of time, seismologists can act quickly to set up a high-resolution monitoring system possibly less than a day for close tracking of aftershock evolution. Taking together the large-N nature, minimal response time, capability for real-time operation, as well as the rich fiber resources around the world, DAS is a promising addition to the modern rapid response toolbox and has the potential to promote an improved understanding of earthquake processes.

Conflict of Interest

The authors declare no conflicts of interest relevant to this study.

Data Availability Statement

The catalog of template events and the broadband data are from the Caltech/USGS Southern California Seismic Network (<https://doi.org/10.7914/SN/CI>) stored at the Southern California Earthquake Data Center (<http://dx.doi.org/10.7909/C3WD3xH1>).

Acknowledgments

The authors are grateful to the instrument and field support provided by Martin Karrenbach, Lisa LaFlame of OptaSense Inc. Thomas Coleman of Silixa Inc. and Andrew Klesh of JPL. We thank the Digital 395 and JPL for providing fiber access promptly after the Ridgecrest earthquake. The work is supported by NSF CAREER Award 1848166, NSF GMG Center at Caltech, and the Braun Trust. Zefeng Li is also supported by USTC Research Funds of the Double First-Class Initiative YD2080002006.

References

- Atef, A. H., Liu, K. H., & Gao, S. S. (2009). Apparent weekly and daily earthquake periodicities in the Western United States. *Bulletin of the Seismological Society of America*, 99(4), 2273–2279. <https://doi.org/10.1785/0120080217>
- Benioff, H. (1935). A linear strain seismograph. *Bulletin of the Seismological Society of America*, 25(4), 283–309. <https://doi.org/10.1785/bssa0250040283>
- Beskardes, G. D., Wu, Q., Hole, J. A., Chapman, M. C., Davenport, K. K., Brown, L. D., & Quiros, D. A. (2019). Aftershock sequence of the 2011 Virginia earthquake derived from the dense AIDA Array and back projection. *Bulletin of the Seismological Society of America*, 109(1), 19–33. <https://doi.org/10.1785/0120180107>
- Catchings, R. D., Goldman, M. R., Steidl, J. H., Chan, J. H., Allam, A. A., Criley, C. J., et al. (2020). Nodal seismograph recordings of the 2019 Ridgecrest earthquake sequence. *Seismological Research Letters*, 91, 3622–3633. <https://doi.org/10.1785/0220200203>
- Cheng, F., Chi, B., Lindsey, N. J., Dawe, T. C., & Ajo-Franklin, J. B. (2021). Utilizing distributed acoustic sensing and ocean bottom fiber optic cables for submarine structural characterization. *Scientific Reports*, 11(1), 5613. <https://doi.org/10.1038/s41598-021-84845-y>
- Dou, S., Lindsey, N., Wagner, A. M., Daley, T. M., Freifeld, B., Robertson, M., et al. (2017). Distributed acoustic sensing for seismic monitoring of the near surface: A traffic-noise interferometry case study. *Scientific Reports*, 7(1), 11620. <https://doi.org/10.1038/s41598-017-11986-4>
- Fan, W., & McGuire, J. J. (2018). Investigating microearthquake finite source attributes with IRIS Community wavefield demonstration experiment in Oklahoma. *Geophysical Journal International*, 214(2), 1072–1087. <https://doi.org/10.1093/gji/ggy203>
- Gulia, L., & Wiemer, S. (2019). Real-time discrimination of earthquake foreshocks and aftershocks. *Nature*, 574(7777), 193–199. <https://doi.org/10.1038/s41586-019-1606-4>
- Hauksson, E., Yoon, C., Yu, E., Andrews, J. R., Alvarez, M., Bhadha, R., & Thomas, V. (2020). Caltech/USGS Southern California Seismic Network (SCSN) and Southern California Earthquake Data Center (SCEDC): Data Availability for the 2019 Ridgecrest sequence. *Seismological Research Letters*, 91(4), 1961–1970. <https://doi.org/10.1785/0220190290>
- Inbal, A., Ampuero, J. P., & Clayton, R. W. (2016). Localized seismic deformation in the upper mantle revealed by dense seismic arrays. *Science*, 354(6308), 88–92. <https://doi.org/10.1126/science.aaf1370>
- Inbal, A., Clayton, R. W., & Ampuero, J.-P. (2015). Imaging widespread seismicity at midlower crustal depths beneath Long Beach, CA, with a dense seismic array: Evidence for a depth-dependent earthquake size distribution: LB ARRAY SEISMIC MONITORING. *Geophysical Research Letters*, 42(15), 6314–6323. <https://doi.org/10.1002/2015GL064942>
- Jousset, P., Reinsch, T., Ryberg, T., Blanck, H., Clarke, A., Aghayev, R., et al. (2018). Dynamic strain determination using fibre-optic cables allows imaging of seismological and structural features. *Nature Communications*, 9(1), 1–11. <https://doi.org/10.1038/s41467-018-04860-y>
- Li, Z. (2018). High-resolution seismic event detection using local similarity for Large-N arrays. *Scientific Reports*, 10.
- Li, Z., & Zhan, Z. (2018). Pushing the limit of earthquake detection with distributed acoustic sensing and template matching: A case study at the Brady geothermal field. *Geophysical Journal International*, 215(3), 1583–1593. <https://doi.org/10.1093/gji/ggy359>
- Lindsey, N. J., Dawe, T. C., & Ajo-Franklin, J. B. (2019). Illuminating seafloor faults and ocean dynamics with dark fiber distributed acoustic sensing. *Science*, 366(6469), 1103–1107. <https://doi.org/10.1126/science.aay5881>
- Lindsey, N. J., Martin, E. R., Dreger, D. S., Freifeld, B., Cole, S., James, S. R., et al. (2017). Fiber-optic network observations of earthquake wavefields. *Geophysical Research Letters*, 44(23), 11792–11799. <https://doi.org/10.1002/2017GL075722>
- Lindsey, N. J., Rademacher, H., & Ajo-Franklin, J. B. (2020). On the broadband instrument response of fiber-optic DAS arrays. *Journal of Geophysical Research: Solid Earth*, 125, e2019JB018145. <https://doi.org/10.1029/2019JB018145>
- Meng, X., & Peng, Z. (2014). Seismicity rate changes in the Salton Sea Geothermal Field and the San Jacinto Fault Zone after the 2010 M w 7.2 El Mayor-Cucapah earthquake. *Geophysical Journal International*, 197(3), 1750–1762. <https://doi.org/10.1093/gji/ggu085>
- Pankow, K. L., Rusho, J., Pechmann, J. C., Hale, J. M., Whidden, K., Sumsion, R., et al. (2021). Responding to the 2020 Magna, Utah, earthquake sequence during the COVID-19 pandemic shutdown. *Seismological Research Letters*, 92(1), 6–16. <https://doi.org/10.1785/0220200265>
- Peng, Z., & Zhao, P. (2009). Migration of early aftershocks following the 2004 Parkfield earthquake. *Nature Geoscience*, 2(12), 877–881. <https://doi.org/10.1038/ngeo0697>
- Reasenber, P. A., & Jones, L. M. (1990). California aftershock hazard forecasts. *Science*, 247(4940), 345–346. <https://doi.org/10.1126/science.247.4940.345>
- Roeloffs, E., & Goltz, J. (2017). The California earthquake advisory plan: A history. *Seismological Research Letters*, 88(3), 784–797. <https://doi.org/10.1785/0220160183>

- Ross, Z. E., Idini, B., Jia, Z., Stephenson, O. L., Zhong, M., Wang, X., et al. (2019). Hierarchical interlocked orthogonal faulting in the 2019 Ridgecrest earthquake sequence. *Science*, *366*(6463), 346–351. <https://doi.org/10.1126/science.aaz0109>
- Ross, Z. E., Trugman, D. T., Hauksson, E., & Shearer, P. M. (2019). Searching for hidden earthquakes in Southern California. *Science*, *364*(6442), 767–771. <https://doi.org/10.1126/science.aaw6888>
- Shelly, D. R. (2020). A high-resolution seismic catalog for the initial 2019 Ridgecrest earthquake sequence: Foreshocks, aftershocks, and faulting complexity. *Seismological Research Letters*, *91*(4), 1971–1978. <https://doi.org/10.1785/0220190309>
- Wang, H. F., Zeng, X., Miller, D. E., Fratta, D., Feigl, K. L., Thurber, C. H., & Mellors, R. J. (2018). Ground motion response to an ML 4.3 earthquake using co-located distributed acoustic sensing and seismometer arrays. *Geophysical Journal International*, *213*(3), 2020–2036. <https://doi.org/10.1093/gji/ggy102>
- Wang, X., Williams, E. F., Karrenbach, M., Herráez, M. G., Martins, H. F., & Zhan, Z. (2020). Rose Parade seismology: Signatures of floats and bands on optical fiber. *Seismological Research Letters*, *91*(4), 2395–2398. <https://doi.org/10.1785/0220200091>
- Wang, X., & Zhan, Z. (2020). Seismotectonics and fault geometries of the 2019 Ridgecrest sequence: Insight from aftershock moment tensor catalog using 3-D Green's functions. *Journal of Geophysical Research: Solid Earth*, *125*(5), e2020JB019577. <https://doi.org/10.1029/2020JB019577>
- Yan, Y., Williams, E. F., & Zhan, Z. (2021). Ambient noise tomography of the near surface using the Ridgecrest DAS array, Abstract Presented at 2021 SSA Annual Meeting, 19-23 April 2021.
- Yu, C., Zhan, Z., Lindsey, N. J., Ajo-Franklin, J. B., & Robertson, M. (2019). The potential of DAS in teleseismic studies: Insights from the Goldstone experiment. *Geophysical Research Letters*, *46*(3), 1320–1328. <https://doi.org/10.1029/2018GL081195>
- Zhan, Z. (2020). Distributed acoustic sensing turns fiber-optic cables into sensitive seismic antennas. *Seismological Research Letters*, *91*(1), 1–15. <https://doi.org/10.1785/0220190112>